Performance evaluation of high-volume evacuation for removing droplets during dental treatment

Chaojie Xing [a, b], Zhengtao Ai [a, b, *], Cheuk Ming Mak [c], Hai Ming Wong [d]

a Department of Civil Engineering, Hunan University, Changsha, 410082, China

b National Center for International Research Collaboration in Building Safety and Environment, Hunan University, Changsha, Hunan, China

c Department of Building Environment and Energy Engineering, The Hong Kong Polytechnic University, Hung Hom, Hong Kong, China

d Faculty of Dentistry, The University of Hong Kong, Pok Fu Lam, Hong Kong Island, Hong Kong, China

Chaojie Xing (chaojiexing@hnu.edu.cn);
Zhengtao Ai (zhengtaoai@hnu.edu.cn) (Corresponding author);
Cheuk Ming Mak (cheuk-ming.mak@polyu.edu.hk);
Hai Ming Wong (wonghmg@hku.hk)

Abstract: The High-volume evacuation (HVE) is commonly employed as a primary source control measure for removing splatter emitted from mouth during dental treatments, but there is still a lack of comprehensive understanding of its efficiency. Based on our previous experiments on the emission characteristics during dental treatments, this study employed Computational Fluid Dynamics (CFD) simulations to investigate the impact of emission parameters (droplet size, emission velocity, emission angle), HVE usage methods (distance between HVE and the droplet release source), and HVE suction flow rates on its removal efficiency. The effect of HVE on Fallow Time (FT) was also examined. Cumulative removal efficiency that accurately reflected the HVE effect was proposed as an evaluation index. It was found that emission velocity was a key factor influencing cumulative removal efficiency. When the distance between HVE and the source was 4 cm, the cumulative removal efficiencies for low-velocity (0.8 m/s), medium-velocity (3.4 m/s), and high-velocity droplets (6.0 m/s) were approximately 97.9%, 73.6%, and 58.0%, respectively. For high-velocity droplets at 6.0 m/s, decreasing the distance between HVE and the source from 4 cm to 2 cm and 1 cm increased the cumulative removal efficiency from 58.0% to 76.7% and 100%. This study was expected to enhance the understanding of HVE performance and provide information on its usage method. It also indicated the strong need for new control measures that could offer broad effective control range and high efficiency in removing high-velocity droplets.

Keywords： High-volume evacuation (HVE); Ultrasonic Scaling Instruments (USI); Powder Jet Handpieces (PJH); High-speed Air Turbine Handpiece (HATH); Fallow time (FT); Computational fluid dynamics (CFD)

1 Introduction

The World Health Organization (WHO) defines Aerosol Generating Procedures (AGPs) as medical, dental, and patient care procedures that generate suspended droplets, posing the risk of infectious disease transmission [1]. AGPs are associated with the use of dental treatment equipment such as Ultrasonic Scaling Instruments (USI), Powder Jet Handpieces (PJH), High-velocity Air Turbine Handpieces (HATH), and the use of a triple syringe [2]. The use of these equipment produced a mixture of blood, saliva, and various microorganisms [1]. Existing studies have found a substantial presence of various pathogens (viruses, bacteria, and fungi) in saliva samples from individuals with respiratory infectious diseases [3-7]. During dental treatments for COVID-19 patients, 418 colony-forming units (CFUs) of the virus were detected per stere on the surrounding surfaces [8]. Due to the high-momentum emissions during dental treatments, splatter could contaminate both air and surfaces throughout the clinic environment [9]. Airborne pollution in clinics originated from splatter with small-size aerosols suspended in the air [10-11], while surface contamination resulted from splatter with large-size droplets deposited on surfaces [12-13]. The suspension and deposition of droplets created a working environment with a high potential for disease transmission [14-15-16]. AGPs could represent significant modes for infection transmission in dental clinics. Studies indicated that even without viruses present in splatters, long-term exposure to inhalable particles could lead to respiratory diseases such as pneumoconiosis [17].

Commonly applied control measures during dental treatments include pre-treatment mouth rinsing with hydrogen peroxide, as well as the use of HVE, rubber dams, and air purifiers. Among these, HVE is a widely used source control measure that relies on negative pressure exhaust ventilation to remove splatters. The removal efficiency of HVE in eliminating splatters has been extensively studied using experimental methods based on human subject and dummy experiments. Experimental setups for evaluating the efficiency of HVE may include standard saliva ejectors, HVE (High Volume Evacuators), EOS (Extra-Oral Suction), or the combination of these instruments. There are four methods for determining the removal efficiency of HVE in removing splatters. The first is the fluorescein method that assesses removal efficiency

based on the deposited area of splatter near the patient's mouth (mainly for large droplets). The second is the particle counter method that determines removal efficiency or quantity (primarily for PM10.0) based on values measured at only one or two points in the air, which inadequately reflects the removal efficiency of HVE. The third is the Petri dish method that assesses removal efficiency based on the quantity of bacterial colonies primarily found in aerosols and small droplets. The fourth is the visualization method that evaluates pollution levels by visualizing the quantity of droplets in a visual plane.

There is a lack of consistent conclusions regarding the removal efficiency of high-suction measures in removing splatters. Some studies have reported a very high removal efficiency of high-suction measures, with the cumulative removal efficiency exceeding 80% [18- 26], implying that these measures are effective in dealing with the emission problem. Some studies indicated that the removal efficiencies range between 20% and 80% [27- 31], and there are some studies suggesting that the removal efficiencies are less than 20% [27, 31- 35]. The significantly different findings obtained in these past studies could be attributed to five key factors: differences in the observed particle size range (particle counters mainly focus on PM10.0, while the fluorescein method focuses on larger droplets deposited on surfaces), variations in particle sampling locations/quantities (splatter is not uniformly distributed), disparities in treatment equipment parameters leading to differences in emission characteristics, differences in HVE parameters (using position, distance, and suction flow rates), and variations in doctors' operating methods and the assistants' proficiency levels. In the end, it remains unclear how these factors impact the removal efficiency of HVE.

Apart from experimental measurements, the efficiency of HVE in removing droplets can be predicted using CFD simulations. However, the boundary conditions of the emission source, including emitted particle size, emission angle, and emission velocity, are important for a reliable and accurate CFD simulations. For the boundary conditions, previous studies have reported different flow rates for the USI. Li et al. [36] measured a flow rate of 50 ml/min and observed the droplet velocities ranging between 4-6 m/s, while Ou et al. [19] reported a flow rate of 36 ml/min with over 65% of droplets emitting below 1.0 m/s. Both Ou et al. [19] and Haffner et al. [37] found that the particle size range was mainly between 12-200 μm. The study conducted by Yuan et al. [26] revealed that the diameter of droplets produced from HATH usage was mainly below 250 μm, with a majority being less than 60 μm. However, these results did not fully consider the impact of teeth position of treatment, saliva volume, and equipment flow rate on emission parameters. Our previous work comprehensively addressed these

influences and provided systematic measurements of particle size distribution, emission angles, and emission velocities for both PJH and USI under various conditions [38], which provided boundary conditions for the present CFD simulations.

Given the inconsistent performance of HVE reported in past studies and the varied boundary conditions of source emission during dental treatments, the present study intended to present a systematical evaluation of HVE performance using CFD simulations based on our measurement of boundary conditions. This study focused on the impact of emission parameters (droplet size, emission velocity, and emission angle), different methods of using HVE (such as varying distances between HVE and the source), and suction flow rate of HVE on its removal efficiency. Additionally, this study examined the impact of using HVE on FT. This study would enhance our understanding of the effectiveness of HVE in controlling splatter, provide information on its usage methods, and recommend directions for developing new control measures.

2 Methods

2.1 Model Description

2.1.1 Dental clinic

The geometry model employed in the present CFD simulations was a representative dental clinic from the periodontal department of Changsha Stomatological Hospital, which measured at 4.5 m × 3.4 m × 3.6 m. The clinic had an upward supply and return air ventilation system with single inlet and outlet. The inlet was equipped with a square diffuser, and the outlet featured a louvered grille, both measuring at 0.3 m × 0.3 m. The dental unit included the dental chair located in the central area of the clinic and an office desk positioned near the wall, as shown in Figure 1.

2.1.2 Treatment Setting

The patient assumed a supine position during dental treatment, as shown in Figure 1. The patient had a body area of 1.74 m^2 and a height of 1.70 m. The used head model was based on an Asian adult male with good oral health to reflect real treatment scenarios, where the patient's mouth was nearly fully open. The standard four-handed operation involved one doctor and one nurse. Both medical workers were seated at approximately 1.3 m in height, with their eyes positioned about 0.4 m away from the patient's mouth. The doctor was positioned at the 9 o'clock direction while the nurse was positioned at the 3 o'clock direction, following a professional dental treatment

layout [39]. To approximate HVE, a cylinder shape was used, and its vent was represented by a circular surface with a diameter of 15 mm [40], placed directly in front of the emission direction.

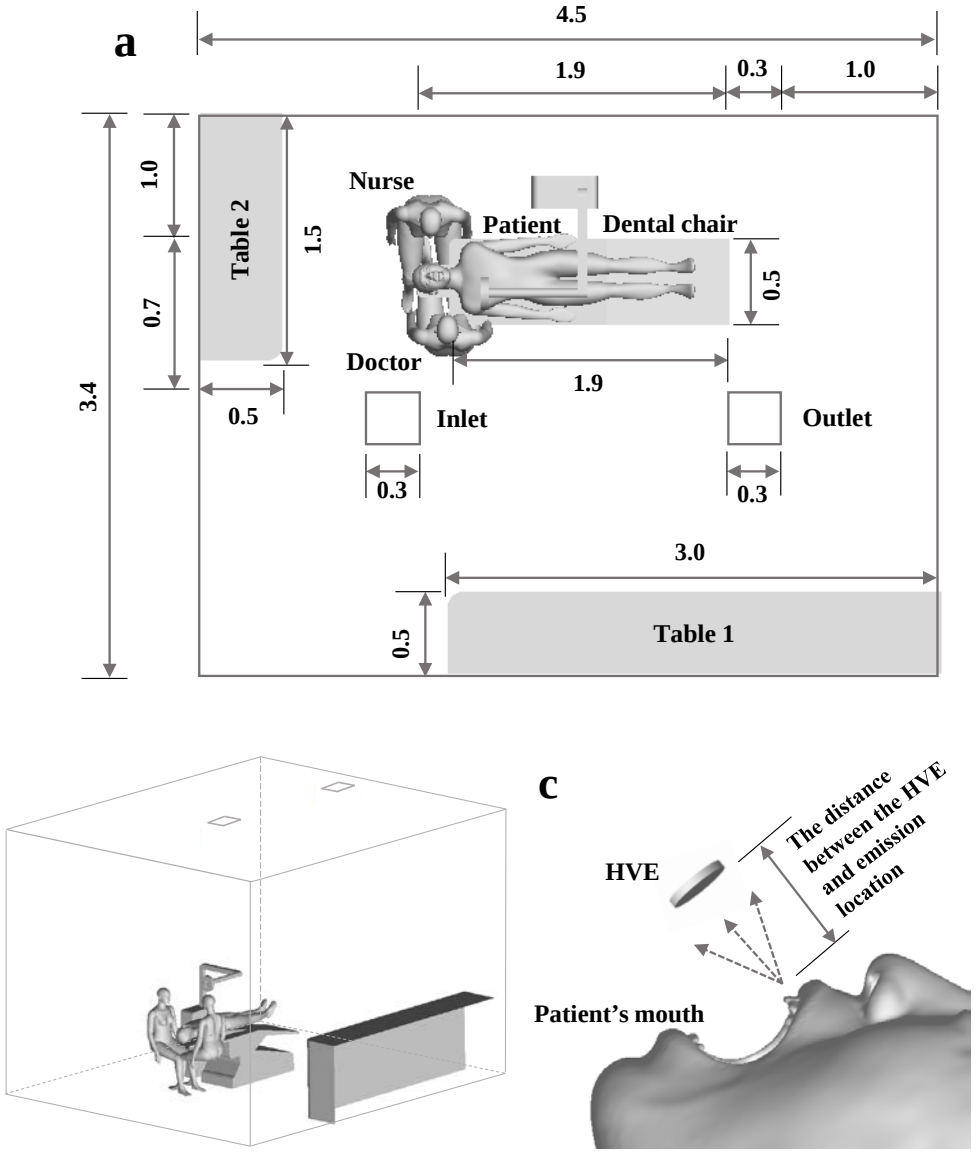

Figure 1 Dental Clinic Floor Plan: (a) Top View (b) Side View (c) Location of HVE (unit: m).

2.2 Numerical setups

To study the behavior of droplets in dental clinic, the CFD methods was employed to study airflow distribution and droplet transmission.

2.2.1 Continuous phase solution

The Reynolds-Averaged Navier-Stokes (RANS) equations were solved to obtain the indoor airflow distribution, eliminating the need for tracking minute fluid movements. The RNG k-ε model, commonly used for solving low Reynolds number

flow problems and demonstrating good performance in complex geometry external flow and droplet transmission, was chosen for turbulent modeling [41-42]. Enhanced wall treatment was applied to describe turbulent characteristics near the walls. The governing equations of mass, momentum, turbulent kinetic energy (k), turbulent dissipation rate (ε), substance transfer, and temperature conservation were discretized to obtain a steady-state solution. The finite volume method was used to discretize the governing equations. Velocity field and pressure field coupling methods were achieved through SIMPLE algorithm. The pressure equation's discretization scheme was based on the PRESTO! algorithm, while a second-order upwind scheme was employed for other equations. Additionally, convergence was achieved when continuity, momentum, turbulence, energy, and species residuals were less than 10e-6. After reaching a steady-state solution, the simulation transitioned into transient mode with a calculation step size set between 1.5e-4 seconds and 1.0 seconds to balance accuracy and computational resources.

CFD simulations conducted in this study utilized the commercial software ANSYS FLUENT 20.0. As control equations for simulation were well-documented in ANSYS Fluent documentation [43], only the droplet evaporation control equation was presented in this study.

2.2.2 Droplet dispersion modeling

The Discrete Phase Model (DPM), commonly used for predicting droplet dispersion in the air [44], was employed to accomplish the prediction of droplet transmission behavior in this study. DPM operated within the Eulerian-Lagrangian framework and utilized a discrete phase model with a one-way coupling scheme to track droplets, determined by their volume fractions [45]. In this study, the released droplets had a very low volume fraction, making the impact of the discrete phase on the continuous phase and interactions among droplets negligible. Accurate prediction of droplet trajectories in the dental clinic relied on considering factors such as droplet resistance, size, and shear. The drag force [46], thermophoretic force [47], and Saffman force [48] were considered in this study. The effect of turbulence on droplet dispersion was modeled using the commonly applied Discrete Random Walk (DRW) model [49].

2.2.3 Evaporation Modeling

Evaporation of droplets occurred when the temperature of the droplet exceeded the vaporization temperature but remained below the boiling temperature. The evaporation process continued until all volatile substances had evaporated. An

evaporation model, which considered both convective and diffusive effects on droplet surfaces, was employed for high rates of vaporization [50]. The governing equation for droplet evaporation was as follows:

$$\frac{dm_p}{dt} = -\pi d_p^2 \frac{ShD}{d_p} \rho \ln\left(\frac{p - p_s}{p - p_\infty}\right) \quad (1)$$

Where m_p represents the mass of droplets (kg), t represents time, d_p represents the diameter of the droplet (m), Sh represents Sherwood number, D represents binary diffusion coefficient (m^2/s), ρ represents fluid density (kg/m^3), P represents total pressure (Pa), and P_S and P_∞ represent partial pressures of water vapor at the surface of the droplet and in air, respectively (Pa).

2.3 Boundary Conditions

The solutions of steady-state and transient were determined by the boundary conditions at the boundaries. The primary boundary conditions in this study were shown in Table 1. The temperature at the air inlet was set to 301.15 K to account for winter conditions. To meet the fresh air requirements in the clinic, the air change rate was set at 7 air changes per hour (ACH). The thermal flux for both patients and medical workers was set to 45 W/m^2 [51] to accurately define the human thermal plume. Since humidity influences droplet evaporation fraction and viral droplet viability in the clinic, it could not be ignored. In CFD simulation, air was modeled as an ideal mixture of air and water vapor.

The relative humidity at the inlet of clinic was set to 50%, while the relative humidity of exhaled air from patients was set to 95% [51]. Droplets consist of volatile and non-volatile substances. The mass fraction of volatile substances in droplets was determined by the evaporated water and the remaining non-volatile droplet nuclei. However, the size of droplet nuclei released during dental treatment was unknown. Based on the findings of Basu et al. [52], it was found that the size of droplet nuclei produced during coughing accounts for only 26% of the initial droplet diameter. Considering that splatter produced during dental treatment contains not only saliva but also blood, teeth fragments, and sanding dust, it can be assumed that the size of droplet nuclei may exceed 26% of the initial droplet diameter. Therefore, we assumed that approximately 64% of the initial droplet diameter represented the size of droplet nuclei, and we set a mass fraction for evaporable droplets at 73.6%.

DPM required that the droplet boundary conditions were set on all surfaces. If droplets were transported to the air inlet, outlet, patient's nose, or the vent of HVE in the dental clinic, they would leave the computational domain and were therefore

designated as "escape". Due to their difficulty in overcoming surface adhesion, droplets in contact with other surfaces were specified as "trap" [53].

Table 1 Details of main boundary condition

Surface/Droplet	Boundary Conditions:
Indoor Walls /Dental Unit	Type: Wall； Heat Flux: 0.
Inlet	Type: Velocity Inlet; Temperature: 301.15 K; Relative Humidity: 50%; Turbulence Intensity: 5%; Viscosity Ratio: 10%.
Outlet	Type: Pressure Outlet.
Patient and Medical workers	Type: Wall; Heat Flux: 45 W/m².
Patient's Nose	Type: Velocity Inlet; Temperature: 310.15 K; Relative Humidity: 95%.
Droplets	Temperature: 301.15 K; Density: 1000 kg/m³; Mass Flow Rate: 0.0013 kg/s.

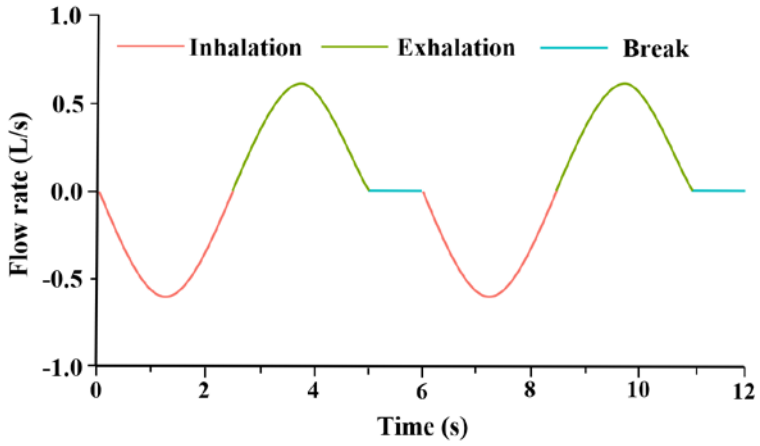

Figure 2 Breathing flow patten.

During dental treatment, it was difficult to completely remove the liquid in the patient's mouth, which might enter their trachea and harm their health if they breathed through their mouth. Therefore, nasal breathing was recommended as the primary mode of respiration with a set breathing rate of 6 l/min [54]. The patient was positioned supine during treatment to correspond with real-life conditions. Nasal breathing occurred through an area of 127 mm² and respiratory flow varied over time as shown in Figure

2. The patient's breathing cycle (6 seconds) consisted of inhalation (2.5 seconds), exhalation (2.5 seconds), and a pause (1.0 seconds). Fluent implemented respiratory conditions using a user-defined function.

Since the initial momentum of droplets in this study was relatively high and the impact of patient respiration on droplets was limited, the influence of the droplet release position on the results could be considered negligible. The droplet release position was set at the maxillary incisors, as shown in Figure 1.

The factors considered in this study included emission velocities, emission angles, droplet size, the distance between HVE and the source, and the suction flow rates of HVE. Based on our previous experiment [38], as shown in Table 2, the parameters of droplets generated by using PJH and USI were influenced by saliva volume on teeth surfaces, teeth position, and equipment flow rate. Taking these factors into account collectively, a comprehensive value following the Rosin-Rammler distribution was adopted to represent the droplets size distribution corresponding to PJH and USI. The primary emission direction under all conditions approximated a cone-shaped release from a point source. The cone release angles ranged between 37° and 71° as shown in Figure 3. The emission velocity near the patient's mouth varied from 0.0 m/s to 6.0 m/s; this also applied to USI. Droplet size distributions of HATH were known based on Yuan et al.'s experiment [26], which were presented in Table 2.

This study combined the parameters of splatter generated by these three types of devices for research purposes. The range of considered emission velocities (0.8 m/s, 3.4 m/s, and 6.0 m/s) and cone half-angles (15°, 25°, and 35°) were extensive in this study since it encompassed the main velocity and angle ranges associated with these three types of devices.

Furthermore, based on the recommendations of medical workers, the distances between HVE and source were set at larger values of 4 cm for complex conditions, with closest distances at 1 cm and closer distances at 2 cm. The suction flow rates for HVE were established as a threshold value of 250 l/min [40], with lower volumes at 150 l/min and higher volumes at 350 l/min. Using these specified parameters, Table 3 presented a total of eighteen Cases.

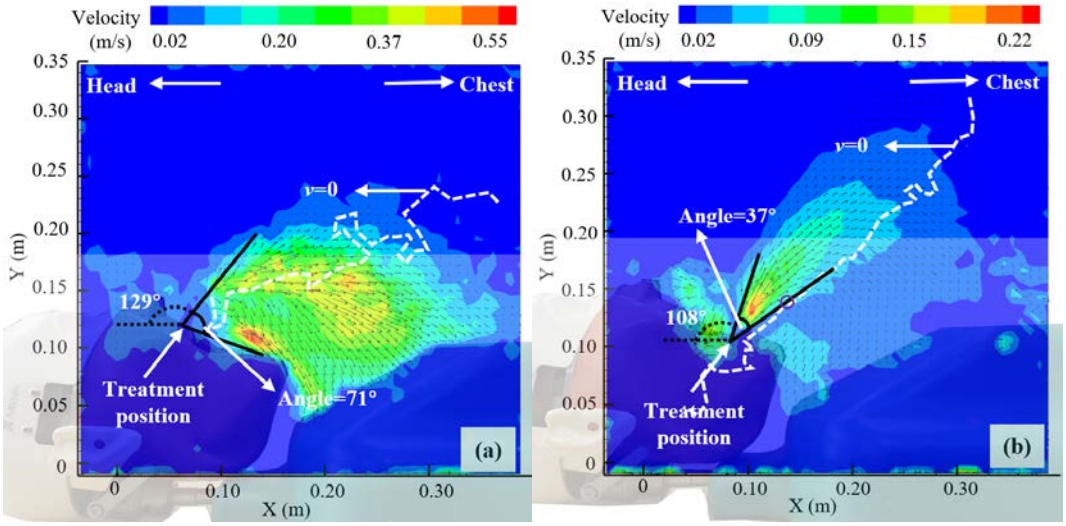

Figure 3 Time averaged distribution of synthetized velocity of droplets generated by using the PJH (based on 200 samples): (a) (80 ml/min of PJH flow rate; 9th tooth), (b) (60 ml/min of PJH flow rate; 24th tooth). Note: the white dashed line (v=0 m/s) represented the v=0 m/s (velocity along Y-axis), which distinguishes the rising and falling areas of droplets.

Table 2 Droplets emission parameters from different dental treatment equipment

Equipment	Emission angle range (°)	Emission velocity range (m/s)	Particle size range (μm)	Average droplet size (μm)	Spread parameter
PJH	37-71	0.0-6.0	10-200	54.95	1.35
USI	25-83	0.0-1.3	10-300	98.93	1.58
HATH	/	/	10-60	24.00	1.83

Table 3 Simulation conditions

Cases	Equipment	Distance between HVE and the source (cm)	Suction flow rates of HVE(l/min)	Emission velocity (m/s)	Emission cone half angle (°)	Time step (s)
1	PJH	4	250	3.4	35	1e-3
2	HATH	4	250	3.4	35	1e-3
3	USI	4	250	3.4	35	1e-3
4	PJH	4	250	0.8	35	5e-3
5	PJH	4	250	6	35	5e-4
6	PJH	4	250	3.4	15	1e-3
7	PJH	4	250	3.4	25	1e-3
8	PJH	2	250	3.4	35	5e-4
9	PJH	2	250	0.8	35	2.5e-3

10	PJH	2	250	6	35	3e-3
11	PJH	1	250	3.4	35	2.5e-4
12	PJH	1	250	6	35	1.5e-4
13	PJH	4	350	3.4	35	1e-3
14	PJH	4	150	3.4	35	1e-3
15	PJH	4	350	6	35	5e-4
16	PJH	4	150	6	35	5e-4
17	USI	2	250	3.4	35	1.0
18	PJH	2	250	0.8	35	1.0

2.4 Model validation

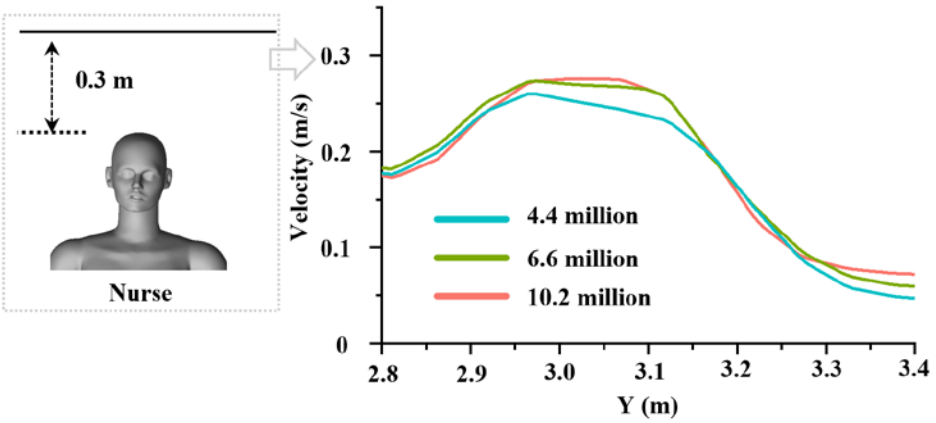

Figure 4 Grid independence test for the dimensionless velocity values.

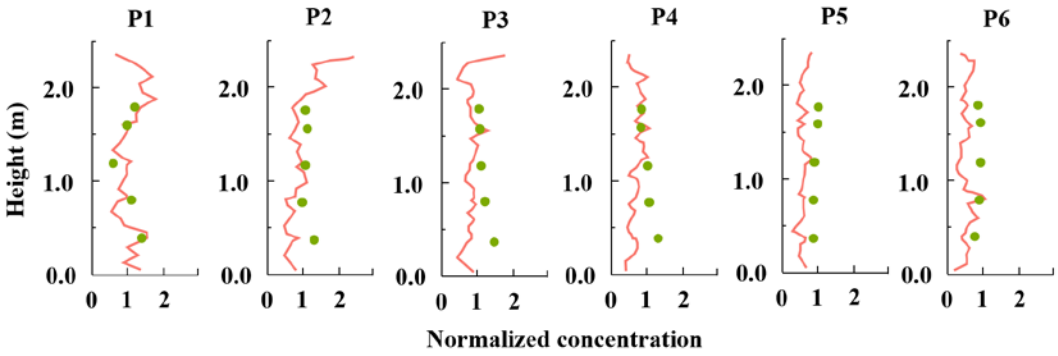

Figure 5 The comparison of simulated and measured particle concentrations.

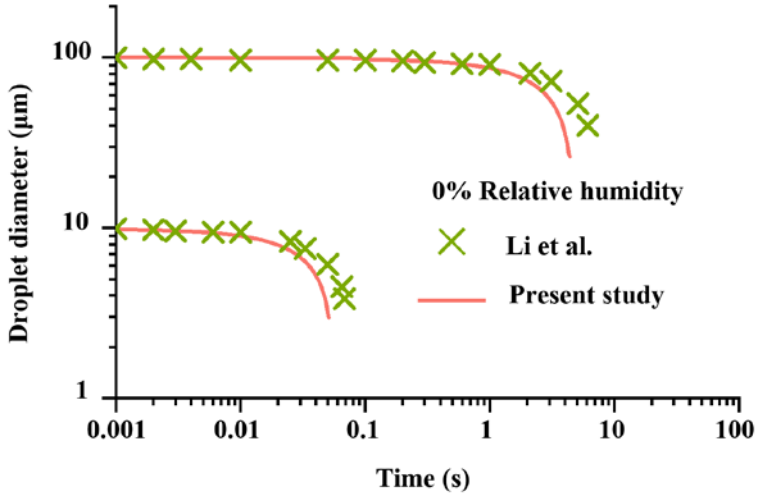

Figure 6 Validation of droplet evaporation.

The grid independence test was conducted using a fine grid (10.2 million), medium grid (6.6 million), and coarse grid (4.4 million) as shown in Figure 4. By comparing the velocity along the monitoring line near the upper part of the patient's mouth, it was observed that the maximum relative deviation for both medium and fine grids was less than 5%, while for the coarse grid, it exceeded 20%. Considering both computational cost and result accuracy, we selected the medium grid for later calculations.

To validate the droplet dispersion model, this study utilized boundary conditions from an experiment conducted by Chen et al. [55] to make predictions and compared them with experimental data as shown in Figure 5. The predicted values aligned well with measured values at most monitoring points. The droplet evaporation model was validated by predicting the change in droplet size over time for freely falling droplets with diameters of 10 μm and 100 μm in a dry environment. These diameters were similar to those used in this study. As shown in Figure 6, the predicted values closely matched the results obtained by Li et al. [56]. Specifically, the droplet size of 10 μm rapidly decreased within 0.1 second, while the droplet size of 100 μm significantly reduced within 10 seconds.

3 Results and analysis

3.1 Airflow field

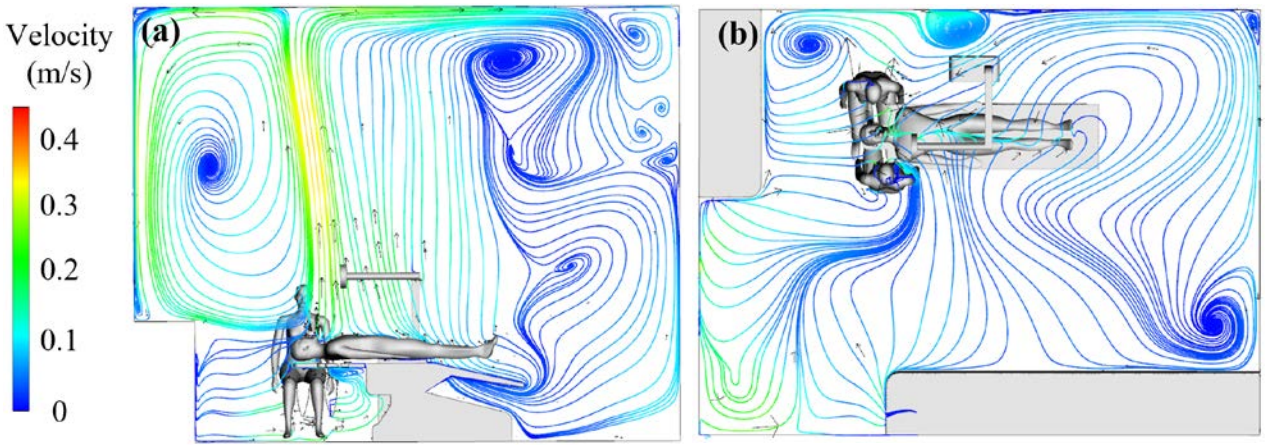

Figure 7 The airflow streamline distribution: (a) x=2.4 m (Vertical to patient's back), (b) z=1.0 m (Patient's upper body, parallel to the patient's back).

The airflow within the dental clinic was the key factor that influences the distribution of droplets. The analysis focused on the velocity distribution in the plane at x=2.4 m and z=1.0 m, where x=2.4 m represented a vertical plane passing through the central axis of the human body, and z=1.0 m represented a horizontal plane parallel to the floor near the upper part of the patient's body, effectively reflecting the flow field distribution around them.

The indoor airflow was influenced by ventilation flow and thermal plumes generated by human bodies. From these two mentioned cross-sections, it could be observed that airflow velocity near the patient's head ranged from 0-0.3 m/s. The presence of vortexes in dental clinics could easily lead to droplet accumulation near doctors' bodies and in corners, forming regions with high concentration. In Figure 7 (a), two distinct large vortexes and several small vortex regions were evident: one large vortex appeared on the left side of the patient's head, 2.3 m above floor level and 0.6 m away from an adjacent wall; another large vortex appeared on their right side, 3.1 m above floor level and 1.5 m away from an adjacent wall. The formation of these two large vortexes was related to upward airflow in upper parts of patients' bodies. Several small vortices appeared in clinic corners due to obstructions caused by dental units or walls. In Figure 7 (b), apart from one vortex near a doctor's body, other vortices were also located close to walls or in corners.

The flow field surrounding HVE under different conditions, which was shown in Figure 8, served as the fundamental background for later analysis of removal efficiency of HVE. This analysis would be combined with the subsequent results.

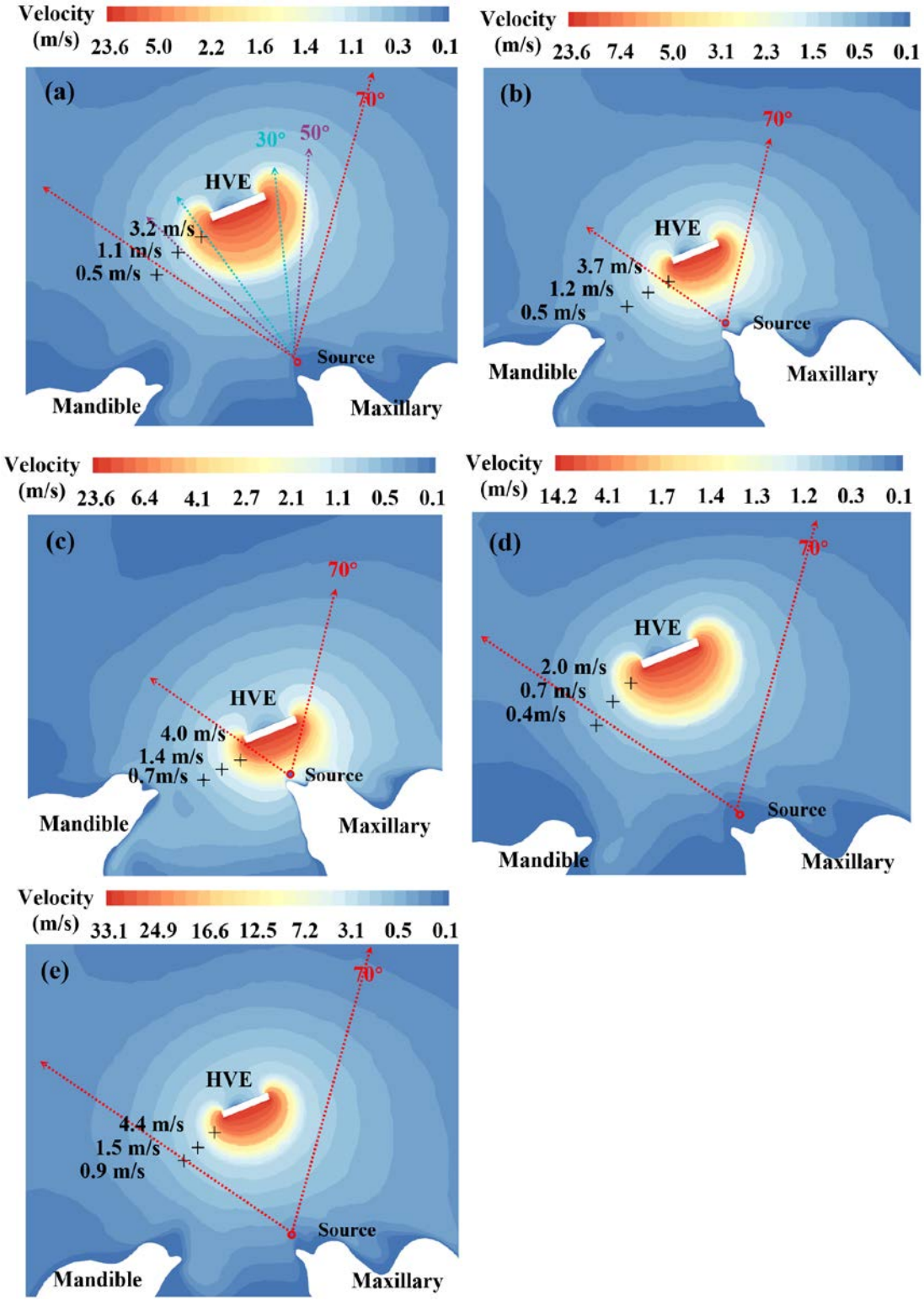

Figure 8 The flow field surrounding HVE. (a): The values in the figure corresponded to Case 1, Case 2, Case 3, Case 4, Case 5, Case 6, and Case 7. The distance between HVE and source was 4 cm, and the suction flow rates of HVE were 250 l/min. (b): The values in the figure corresponded to Case 8, Case 9, Case 10, Case 17, and Case 18. The distance between HVE and source was 2 cm, and the suction flow rates of HVE

were 250 l/min. (c): The values in the figure corresponded to Case 11 and Case 12. The distance between HVE and source was 1 cm, and the suction flow rates of HVE were 250 l/min. (d): The values in the figure corresponded to Case 14 and Case 16. The distance between HVE and source was 4 cm, and the suction flow rates of HVE were 150 l/min. (e): The values in the figure corresponded to Case 13 and Case 15. The distance between HVE and source was 4 cm, and the suction flow rates of HVE were 350 l/min.

3.2 Initial emission parameters of droplets

The differences in splatters generated by using USI, PJH, and HATH included variations in emission velocity, emission angles, and droplet sizes. Firstly, this study aimed to clarify the impact of differences in droplet size on the removal efficiency of HVE. Subsequently, the effects of emission velocity and angles on removal efficiency were studied based on the diameters of droplets generated from using PJH. Examining these parameters contributed to a comprehensive assessment of the removal efficiency of HVE in removing splatter.

3.2.1 Droplet size

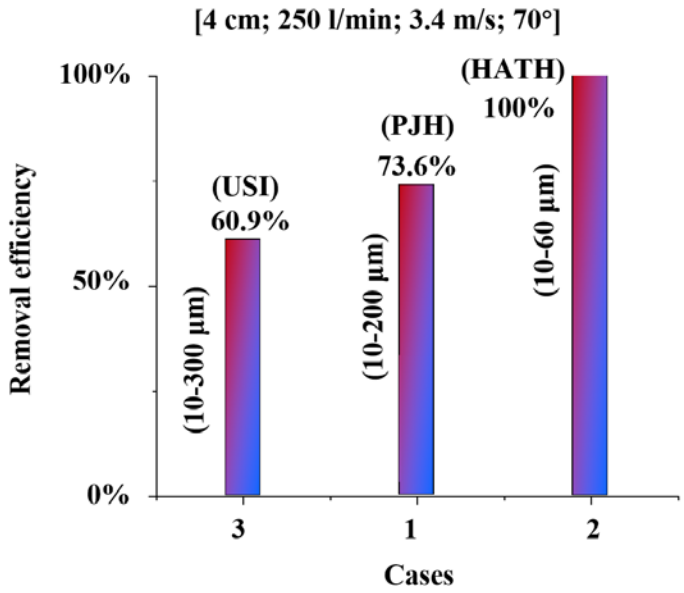

Figure 9 The distribution of removal efficiency of HVE during the use of USI, PJH, and HATH. Notably, the "4 cm" represented the distance between HVE and the source; "250 l/min" represented the suction flow rate of HVE; "3.4 m/s" represented emission velocity; "70°" represented emission angles.

The impact of the droplet size distribution corresponding to USI, PJH, and HATH

on the removal efficiency of HVE was shown in Figure 9. The cumulative removal efficiency of HVE stabilized rapidly within a short duration. The average sizes of the droplets corresponding to three equipment were 98.9 μm, 55.0 μm, and 24.0 μm, with droplet size ranges of 10-300 μm, 10-200 μm, and 10-60 μm respectively. As shown in Figure 9, the cumulative removal efficiency of HVE was highest for HATH (100%), followed by PJH (73.6%) and USI (60.9%). This variation in removal efficiency was correlated with droplet size as larger droplets possess greater momentum enhancing their ability to escape from HVE.

3.2.2 Emission velocity of droplet

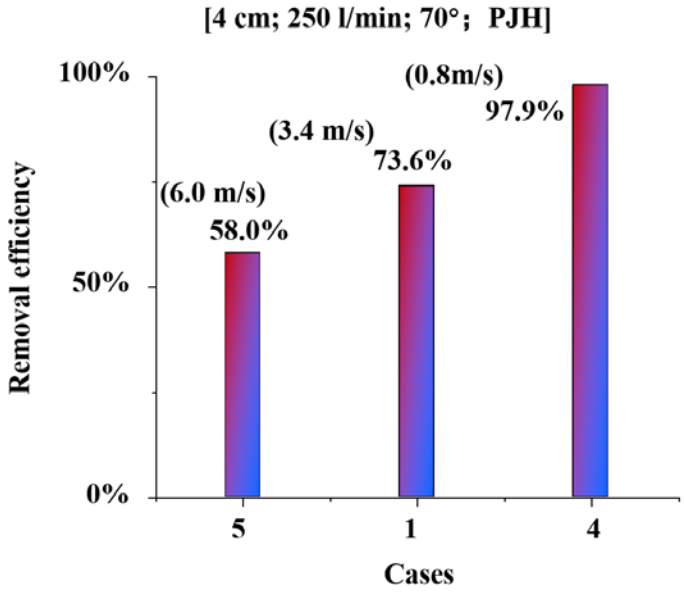

Figure 10 The distribution of removal efficiency of HVE with the emission velocities of 0.8 m/s, 3.4 m/s, and 6.0 m/s. Notably, the "4cm" represented the distance between HVE and the source; "250 l/min" represented the suction flow rate of HVE; "0.8 m/s, 3.4 m/s, 6.0 m/s" represented emission velocity; "70°" represented emission angles.

As shown in Figure 10, the higher the velocity of droplet, the lower the cumulative removal efficiency of HVE. The cumulative removal efficiency for medium-velocity (3.4 m/s) droplets was 73.6%, ranging from 97.9% (for 0.8 m/s droplets) to 58.0% (for 6.0 m/s droplets). This analysis indicated that using HVE alone could effectively remove most low-velocity droplets, but its efficiency in removing medium-velocity and high-velocity droplets was poor. Combining Figure 8 (a), it could be observed that the range of velocity fields with a magnitude greater than 0.5 m/s was larger, while the range of velocity fields exceeding 3.2 m/s was smaller. This implied that HVE had a wider control range for low-velocity droplets and a narrower control range for high-

velocity droplets.

3.2.3 Emission angles of droplets

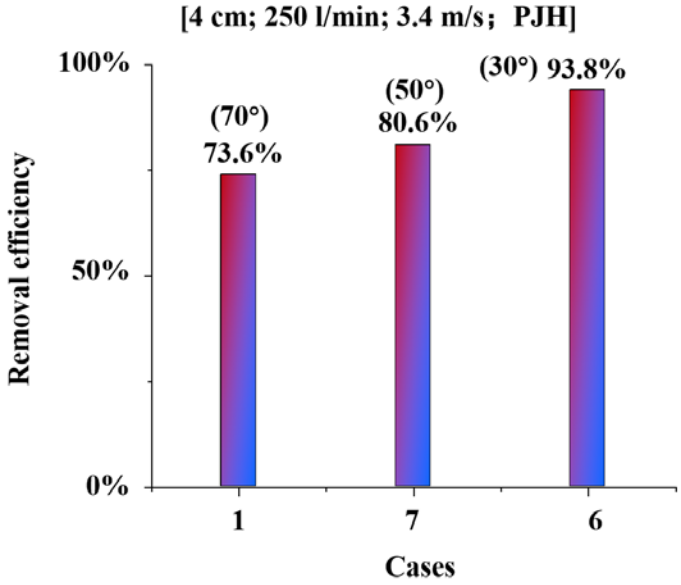

Figure 11 The distribution of removal efficiency of HVE with the emission angles of 30°,50°, and 70°. Notably, the "4cm" represented the distance between HVE and the source; "250 l/min" represented the suction flow rate of HVE; "3.4 m/s, 6.0 m/s" represented emission velocity.

As shown in Figure 11, when the emission angles were 70°, 50°, and 30°, the cumulative removal efficiencies of HVE were 73.6%, 80.6%, and 93.8% respectively. This indicated that the cumulative removal efficiency decreased as the emission angles increased within the range of 30-70°. Combining Figure 8 (a), this was because as the emission angle decreased, droplet diffusion became less sufficient, resulting in more droplets being within the effective control range of HVE.

3.3 Distance between HVE and source

If the suction flow rates of HVE remain constant, the only adjustable parameter in using HVE might be the distance between it and the source. Combining with Figure 10, for high velocity (3.4 m/s, 6.0 m/s) droplets, when the distance between HVE and source was 4 cm, the minimum removal efficiency was 58.0%. Therefore, it was necessary to assess the removal efficiency of HVE at a closer distance to clarify its impact on results. This would help make recommendations on optimal distances for using HVE.

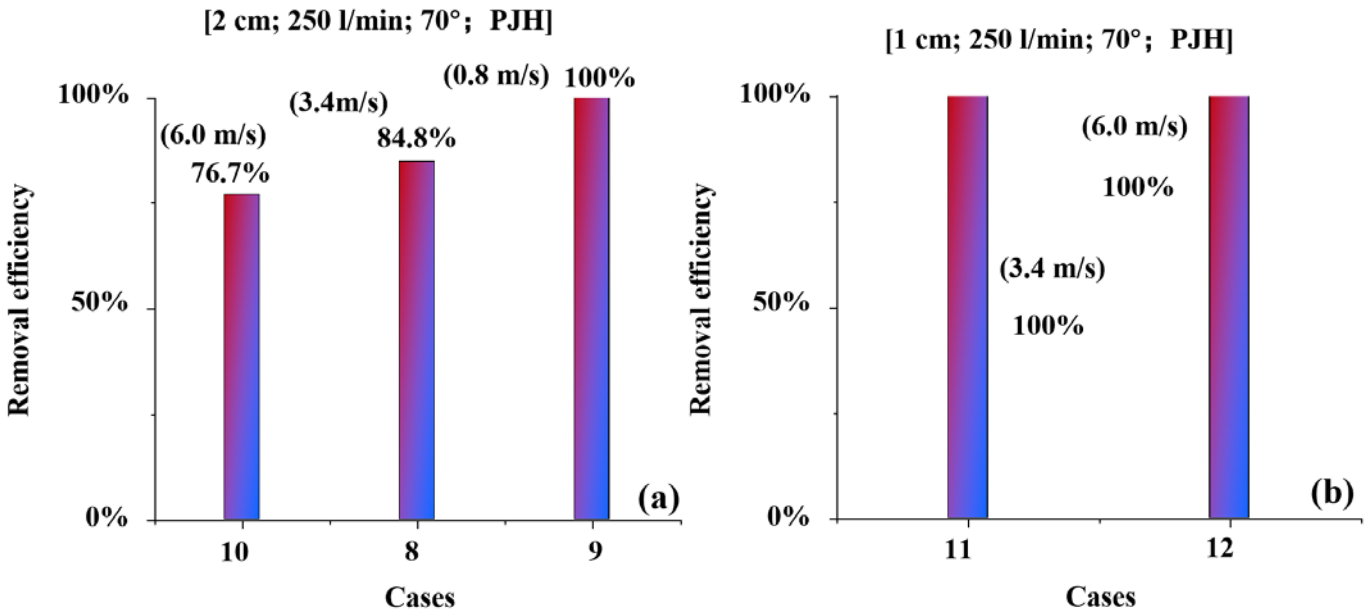

Figure 12 The distribution of removal efficiency of HVE with the distance between HVE and the source ranging from 1 to 2 cm. Notably, "250 l/min" represented the suction flow rate of HVE; "0.8 m/s, 3.4 m/s, 6.0 m/s" represented droplet emission velocity; "70°" represented droplet emission angles.

Combining Figure 10 and Figure 12 (a), the removal efficiency of droplets with velocities of 0.8 m/s, 3.4 m/s, and 6.0 m/s increased from 97.9%, 73.6%, and 58.0% to 100%, 84.8%, and 76.7% respectively, as the distance between HVE and the source decreased from 4 cm to 2 cm. This indicated that reducing the distance was beneficial for improving the removal efficiency, as it allowed for complete removal of all droplets at a velocity of 0.8 m/s but fell short in removing droplets at velocities of both 3.4 m/s and 6.0 m/s.

According to Figure 12 (b), by decreasing the distance from 2 cm to 1 cm, high velocity (6 m/s) droplets could be completely removed. Combining Figure 8 (a), (b), and (c), it could be inferred that as the distance between HVE and the source decreased, the effective control angle of HVE on emitted droplets increased. When reaching HVE, droplets released in a cone shape had not fully dispersed; thus, they could not be completely removed. To our knowledge, specific guidelines for the distance at which HVE should be used during dental treatment were not clearly defined, and medical workers often rely on experience. Based on the present study, it was recommended to maintain within 1 cm from the source when using HVE.

3.4 Suction flow rates of HVE

In real-life dental treatment, it is difficult to achieve 1 cm between HVE and the

source. Therefore, this study investigated the impact of increasing suction flow rates on the removal efficiency of HVE at a distance of 4 cm for high-velocity droplets in order to provide suggestions for optimizing HVE.

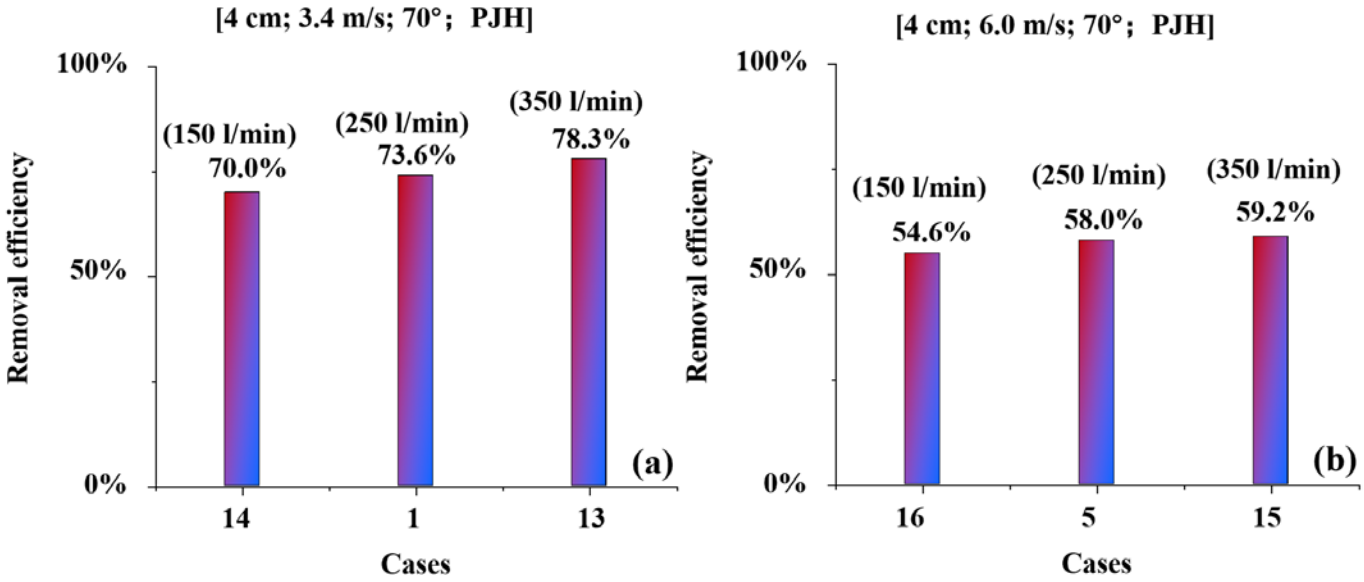

Figure 13 The distribution of removal efficiency of HVE with the suction flow rate of HVE ranging from 150-350 l/min. Notably, the "4cm" represented the distance between HVE and the source; "3.4 m/s, 6.0 m/s" represented emission velocity of droplet; "70°" represented droplet emission angles.

The cumulative removal efficiency of HVE increased when there was an increase in suction flow rates, as depicted in Figure 13 (a). For instance, when the velocity of droplet was 3.4 m/s, changing the suction flow rates from 250 l/min to 350 l/min resulted in the cumulative removal efficiency of HVE increasing from 73.6% to 78.3%. Similarly, the cumulative removal efficiency decreased from 73.6% to 70.0% when the flow rate of HVE was reduced to 150 l/min. As shown in Figure 13 (b), at a velocity of droplet of 6.0 m/s, raising the suction flow rates from 250 l/min to 350 l/min, or reducing it to 150 l/min, led to corresponding changes in cumulative removal efficiency from 58.0% to 59.2% and 54.6%, respectively.

The analysis above indicated that, although there was a positive correlation between suction flow rates and cumulative removal efficiency, a substantial increase in suction flow rates did not lead to a significant improvement in cumulative removal efficiency. Enlarging the suction flow rates of HVE still proved ineffective in removing high-velocity droplets.

Combining Figure 8 (d) and (e), it could be inferred that increasing or decreasing the suction flow rate of HVE would result in an increase or decrease in the airflow

velocity around HVE. However, it was easy to deduce that there was no significant change in the velocity range above 3.4 m/s and 6.0 m/s. This also indicated that the capturing capability of HVE for high-velocity droplets (3.4m/s, 6.0m/s) remained unchanged. Currently, larger suction flow rates of HVE implied greater noise, which could contribute to patient discomfort. Therefore, under the condition of constant HVE diameter, it was not recommended to increase the suction flow rates of HVE to enhance cumulative removal efficiency.

3.3 Simulation time and Fallow time

To further optimize control measures during dental treatment, it was necessary to assess the impact of high and low removal efficiencies of HVE on fallow time. The accuracy of calculations was not crucial for this purpose. Even with abundant computational resources, using a time step magnitude of 10e-3 could take several months to calculate a duration of 30 minutes. In real-life dental treatment, splatter was extremely complex due to changing factors such as emission direction, velocity, and the habits of medical workers. These variations led to continuous fluctuations in the efficiency of HVE. Therefore, using a time step size of 10e-3 might be meaningless in real-life scenarios. Based on these reasons, the time step size was set at 1.0 second.

The above analysis indicated that the cumulative removal efficiency of HVE was significantly higher for low-velocity droplets compared to high-velocity ones. During real-life dental treatments, air-powder-polishing typically lasted for 5 minutes, while ultrasonic scaling lasted for 30 minutes [57]. Therefore, during air-powder-polishing, where relatively low-velocity droplets were generated in a short duration, it represented a condition with lower contamination levels and superior removal efficiency of HVE. On the other hand, ultrasonic scaling involved high-velocity and long-duration droplet generation, resulting in higher contamination levels and less effective control by HVE. Investigating these two conditions was more conducive to revealing the impact of using HVE on FT as shown in Figure 14 and Figure 15. FT was defined as the time required for reducing suspended droplet quantity in dental clinics to a safe level [58].

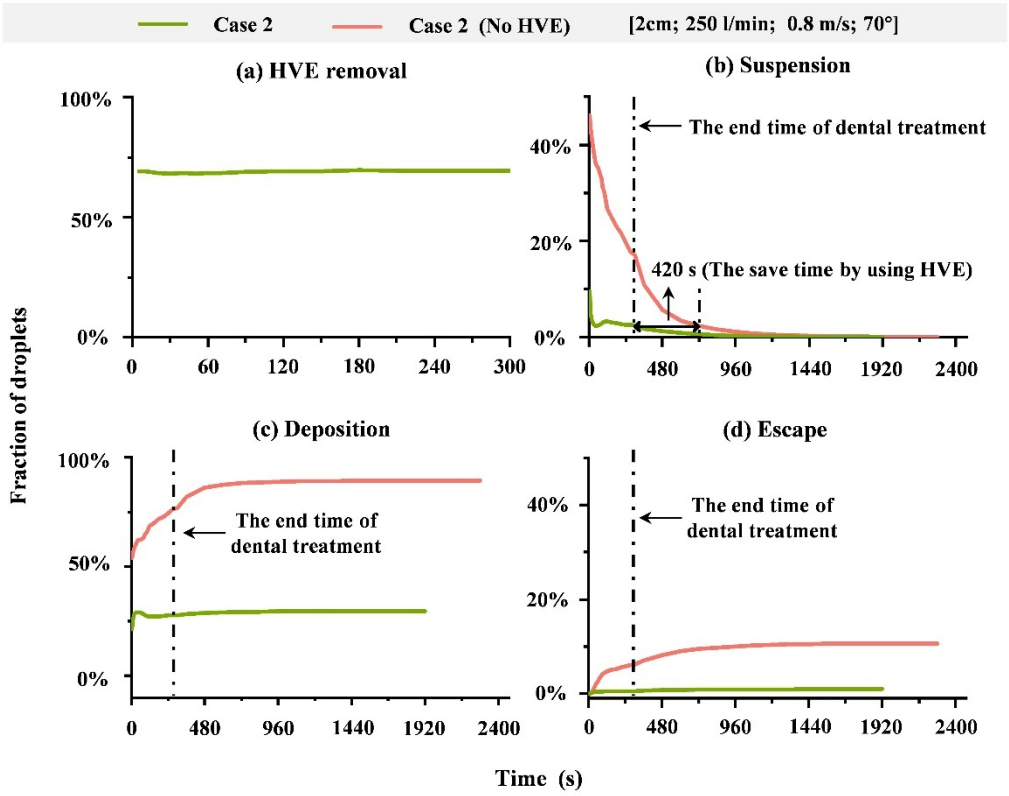

Figure 14 The distribution of droplet number fractions during air-powder-polishing for 5 minutes and FT: (a): HVE removal; (b): Suspension; (c): Deposition; (d): Escape.

The impact of treatment duration on droplet fate was evaluated by analyzing data from 0-300 seconds. From Figure 14 (a), it could be observed that the cumulative removal efficiency of HVE stabilizes at around 69.0%.

In addition to being removed by HVE, droplets could undergo deposition, escaped through ventilation vents, or remained suspended. The fate of droplets was influenced by factors such as airflow patterns within the dental clinic, initial droplet momentum, and forces acting on them. Factors that affected droplet deposition include their initial momentum and the forces acting on them. The cumulative suspension fraction, deposition fraction, and ventilation escape fraction are defined as the proportions of total released droplets that were suspended, deposited, or ventilated escaped respectively. It was currently widely accepted that inhaling virus-containing droplets or contacting with virus-laden droplets deposited on surfaces could lead to disease transmission. Study on the use of HVE and its impact on the fate of droplets was valuable for evaluating its effectiveness in reducing cross-infection risks.

Figure 14 (b) and (c) indicated that within 300 seconds, droplets had sufficient

time to settle. Even without using HVE, the cumulative suspension rate rapidly decreased to 17.0% within 300 seconds, while the cumulative deposition fraction increased rapidly to 76.8%. However, using HVE significantly reduced both the cumulative suspension fraction and deposition fraction to only 2.5% and 29.0%, respectively. Additionally, Figure 14 (d) showed that within a span of just 300 seconds, the cumulative ventilation escape fraction reached around 6.2%. Nevertheless, with the implementation of HVE, this value was reduced drastically to approximately only 0.4%.

The cumulative escape fraction within 120 seconds did not exceed 3.5%, indicating that dental clinic ventilation could not timely and efficiently remove droplets like HVE (source control measures). Furthermore, it was worth noting that the cumulative escape fraction was also influenced by the duration of treatment, as demonstrated in Figure 15 during long-duration simulations.

Analyzing data beyond 300 seconds to assess the impact of HVE on FT. At the 300 seconds, droplet generation stopped and HVE was not used. Suspended droplets gradually decreased over time. Li et al. [59] defined the duration of FT as the time needed for the concentration of suspended droplets to reduce to background levels after dental treatment was completed. However, achieving a complete reduction of suspended droplet quantity to zero, corresponding to background levels, was challenging in CFD simulations. Liu et al. [60] used assumed droplet quantities in simulations to calculate infection risk in dental clinics and determine FT durations. Since the actual quantity of droplets generated during dental treatment was unknown, there might be variations from real-life results. As shown in Table 4 and Figure 14, simulated suspended droplet quantity gradually decreased over time but with an increasing amount of time required for reducing the same quantity of droplets constantly. Achieving a reduction to zero suspended droplets within a dental clinic took several hours, making practical implementation of FT unrealistic. Therefore, we defined the duration of FT as the time required for almost no further change in suspended droplet quantity.

Table 4 The time required for the cumulative suspension fraction of droplets to decrease from 10.0% to a certain value after treatment cessation.

Cumulative suspension fraction	10.0%	8.0%	6.0%	4.0%	2.0%	0.1%
Time (s)	0	33	97	190	393	1520

Combining Figure 14 and Table 4, we assumed that the quantity of suspended droplets stopped varying with time once it decreased to 0.1% of the total droplets. Calculated from the end of the dental treatment, the times required to reach this

threshold with and without the use of HVE were 1020 seconds and 1520 seconds, respectively. This time difference (420 seconds) was comparable to the time savings achieved by using HVE, as indicated in Figure 14 (b). Normalizing based on conditions without HVE, its use reduced FT to only 68.0% compared to background conditions (No using HVE).

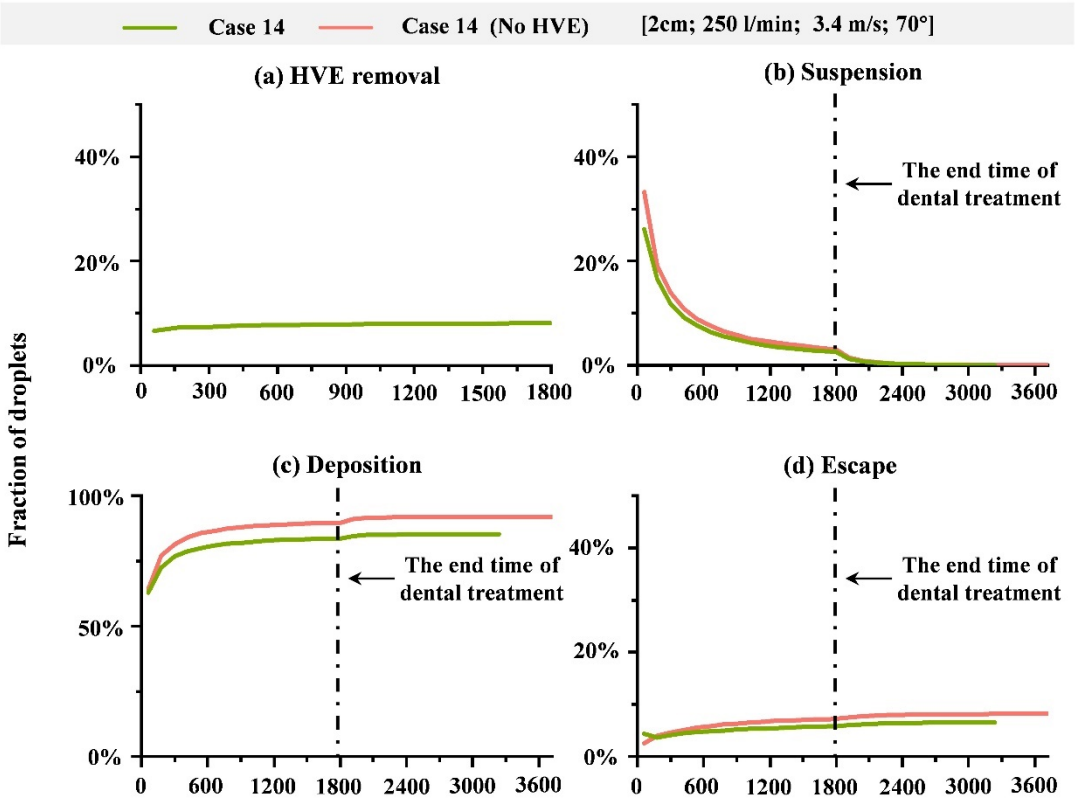

Figure 15 The distribution of droplet number fractions during ultrasonic scaling for 30 minutes and FT: (a): HVE removal; (b): Suspension; (c): Deposition; (d): Escape.

The data from 0 to 1800 seconds was analyzed to assess the impact of treatment duration on droplet fate. As shown in Figure 15 (a), the cumulative removal efficiency of HVE remained stable at about 8.1%. However, when the treatment duration reached 1800 seconds, there was no significant reduction in the cumulative suspended droplet fraction with continued utilization of HVE, only decreasing from 3.1% to 2.5%. This phenomenon could be attributed to an extended treatment time that allowed sufficient time for droplets to settle, resulting in a lower cumulative suspended fraction.

The distribution of suspended droplets in the dental clinic was depicted in Figure 16. Droplets generated near the patient's mouth initially moved along the indoor airflow toward the upper part of the clinic and then dispersed into the surrounding environment.

As shown in Figure 16 (a) and (b), irrespective of using HVE, at the initial moment (60 seconds), droplets were primarily concentrated around the patient's mouth area and upper region. With an extended treatment time to 900 seconds (Figure 16 (c) and (d)), droplets had dispersed throughout the entire clinic.

At the end of the treatment time, namely at 1800 seconds (Figure 16 (e) and (f)), the number of suspended droplets in the clinic reached its maximum. However, compared to 900 seconds, there was only a slight increase in the number of droplets within the clinic, which could be attributed to nearly equal production and removal of droplets. At 2520 seconds (Figure 16 (g) and (h)), which was 720 seconds after the end of treatment, the quantity of suspended droplets significantly decreased but they were approximately evenly distributed throughout the entire space. Additionally, only droplets with diameters of 6.4 μm and 16.1 μm suspended in the clinic. At 3240 seconds (Figure 16 (i) and (j)), corresponding to 1440 seconds after the end of treatment, a small quantity of droplets with a diameter of 6.4 μm still suspended in the clinic and these droplets were challenging to remove through deposition and ventilation methods.

To encompass the respiratory zones of medical workers in various sitting, standing, and working postures within the dental clinic, this study defined the height range from 1.0 m to 1.8 m above the floor as the respiratory zone for medical workers. For all Cases considered in this study, 30 seconds after droplet release, approximately 20% of the total suspended droplets remained within the respiratory zone. This phenomenon occurred due to the smaller size of suspended droplets, which were significantly influenced by indoor airflow. Since the distribution of indoor airflow remained consistent under different conditions, there was a similar fraction of droplets in the respiratory zone compared to total suspended droplets.

With the treatment duration increasing, the use of HVE reduced the cumulative deposition fraction. At 1800 seconds, it decreased from 89.7% to 83.6%. According to Figure 15 (d) at 1800 seconds, using HVE also reduced the cumulative escape fraction from 7.2% to 5.8%. This indicated that using HVE slightly lowers this fraction and further emphasized that droplets primarily undergo deposition, followed by suspension and escape.

Clarifying the fraction of deposition and the main deposition locations could guide the focus areas for surface disinfection. In Case 17 and Case 18, the ranking of cumulative deposition fraction on various surfaces was as follows: surfaces near the patient's mouth area (patient + medical workers + dental chair) > floor > relatively distant surfaces (table + door + window + other walls). This indicated that surfaces around the patient's mouth area were considered as main deposition areas, which was

consistent with existing research [54].

Table 5 The time required for the cumulative suspension fraction of droplets to decrease from 2.53% to a certain value after treatment cessation.

Cumulative suspension fraction	2.53%	1.23%	0.26%	0.08%	0.03%
Time (s)	0	120	600	1080	1440

Analyzing data beyond the 1800 seconds to assess the impact of HVE on FT, we combined information from Table 5 and Figure 15. The cumulative suspension fraction of droplets decreased to 0.03%, showing minimal variation over time. Calculated from the end of treatment, it took 1440 seconds for conditions with HVE usage and 1560 seconds without HVE usage to reach this value. Normalizing these values, the use of HVE reduced FT to 92.3% compared to the background condition. In summary, HVE reduced FT within a range of 68.0%-92.3% compared to the background condition.

Remarkably, this range closely aligned with the experimental results of Li et al. [59] (68.6%-88.9%), providing additional evidence for the reliability of our findings.

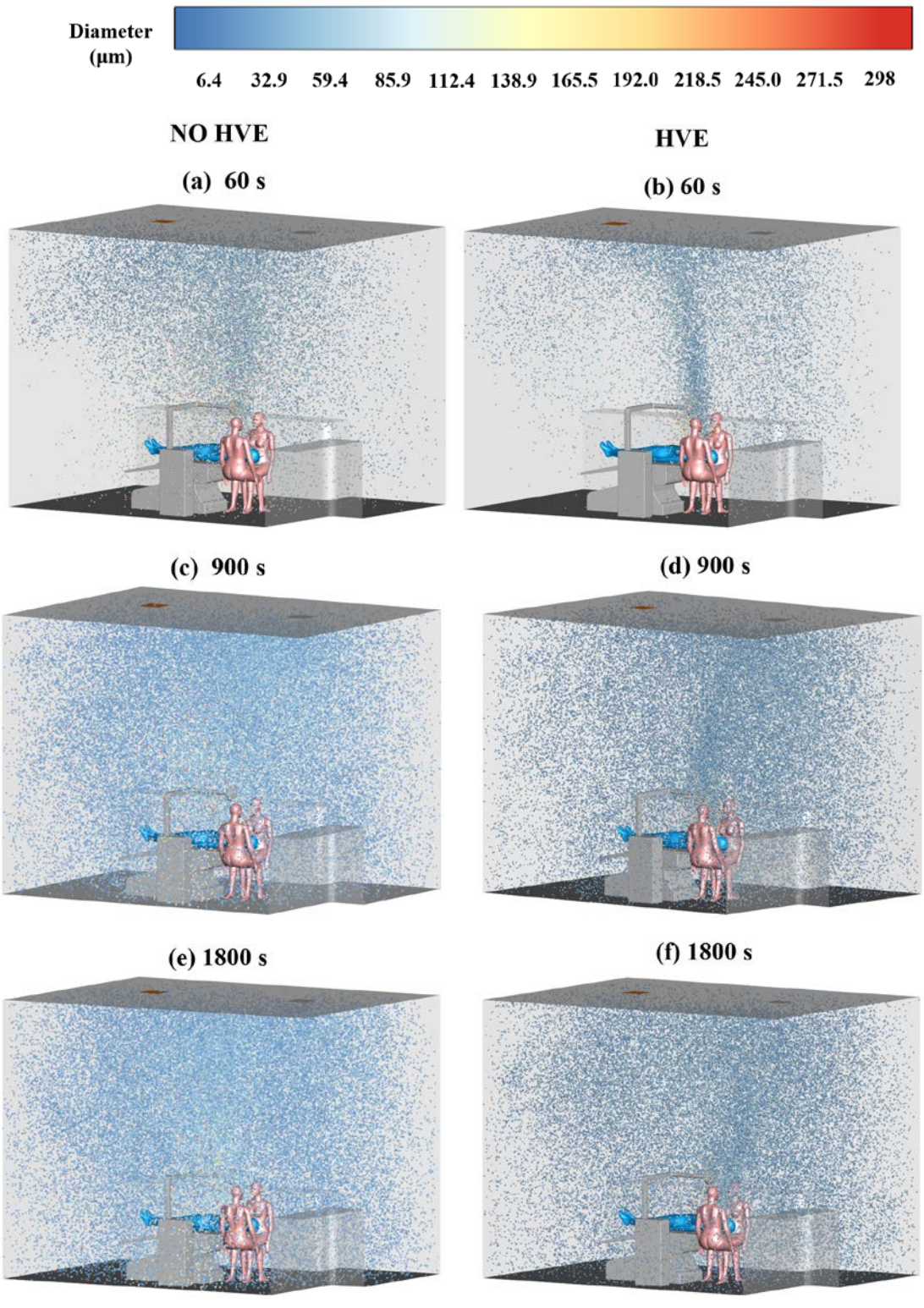
Diameter (μm)
6.4 32.9 59.4 85.9 112.4 138.9 165.5 192.0 218.5 245.0 271.5 298
NO HVE
HVE
(a) 60 s
(b) 60 s
(c) 900 s
(d) 900 s
(e) 1800 s
(f) 1800 s

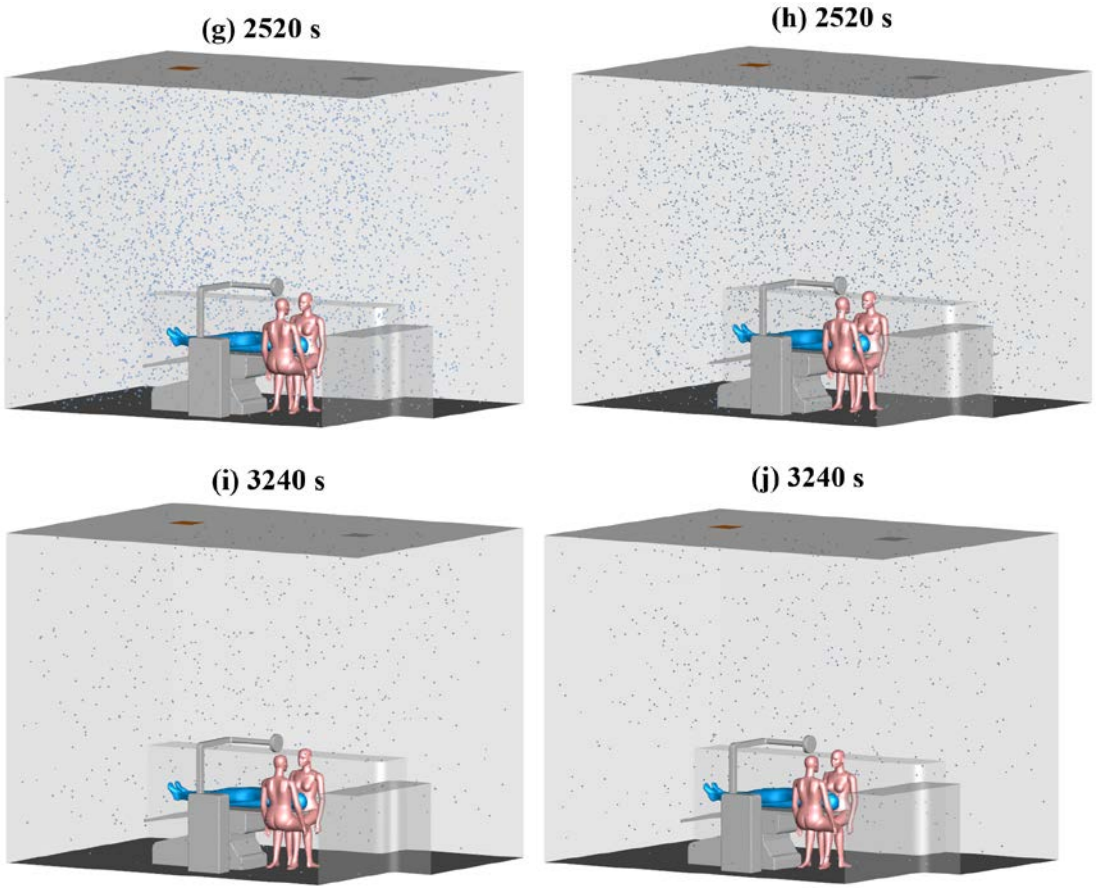

Figure 16 Distribution of suspended droplets during ultrasonic scaling for 30 minutes and FT: NO HVE: (a) Ultrasonic scaling for 60 seconds; (c) Ultrasonic scaling for 900 seconds; (e) Ultrasonic scaling for 1800 seconds; (g) Cessation of ultrasonic scaling for 720 seconds; (i) Cessation of ultrasonic scaling 1440 seconds. HVE using: (b) Ultrasonic scaling for 60 seconds; (d) Ultrasonic scaling for 900 seconds; (f) Ultrasonic scaling for 1800 seconds; (h) Cessation of ultrasonic scaling for 720 seconds; (j) Cessation of ultrasonic scaling for 1440 seconds.

4 Discussion

The impact of droplet size, emission velocity, emission angle, distance between HVE and the source, and the suction flow rates of HVE on its efficiency were firstly studied in this study, and the influence of using HVE on FT was further investigated. The findings contributed to a better understanding of HVE performance, provided guidance for its usage, and highlight challenged in controlling splatter during dental treatment. Consequently, it was recommended that new control measures be developed.

The results of this study indicated that smaller emission angles and velocities, as well as shorter distances for using HVE, resulted in higher removal efficiency. This finding seemed to be obvious and it could also explain the observed upper limits (70.0% or

96%) and lower limits (20% or 38%) of removal efficiency in previous experimental studies [20, 31].

When the removal efficiency of HVE reached 69.0%, 31.0% of droplets were not removed by HVE and escaped into the clinic. However, the fallow time did not decrease to 31.0% of background conditions (No using HVE) but remained at 68.0%. This means that even though HVE maintains a high removal efficiency, the reduction in fallow time is not ideal. Therefore, it is necessary to consider developing source control methods that are effective even with larger diameters and longer distances of action, such as applying miniaturized vortex ventilation devices during dental treatment. Although larger diameter EOS has recently appeared on the market, their principle still relies on negative pressure ventilation. Compared to EOS, vortex ventilation devices offer advantages such as a greater range of action and efficient pollutant removal without affecting the operations of medical workers.

Furthermore, it should be noted that there was no significant difference in fallow time between the cases with 5 minutes and 30 minutes dental treatments under the background conditions. The durations of fallow time for the two cases were measured to be 1520 seconds and 1560 seconds, respectively. This fact might be attributed to the adequate settling time for droplets generated during the longer dental treatment and the almost exclusive reliance on ventilation rate for their removal mechanism. Based on this observation, it might reasonably be predicted that the duration of dental treatment did not affect the required fallow time when it exceeded 5 minutes.

As the fraction of evaporable droplets during dental treatments was unknown, this study assumed a droplet core size (namely, droplet nuclei) equal to 64% of the initial droplet diameter. To assess the impact of droplet core size on the results, one comparative case was added where the only difference from Case 1 was assuming a droplet core diameter equal to 26% of the initial droplet diameter [52], corresponding to coughing conditions. In this comparative case, the cumulative removal efficiency of HVE was 73.8%, which was close to that of Case 1 (73.6%). It was evident that the influence of the evaporation ratio on cumulative removal efficiency of HVE could be negligible.

Considering that droplets smaller than 10 μm were more likely to remain suspended in the air and increase the risk of infection, a comparative case was added where the only difference from Case 1 was that the minimum droplet size was reduced to 1 μm. In this comparative case, the cumulative removal efficiency of HVE was 73.7%. Compared to the removal efficiency of Case 1 (73.6%), the relative error was less than 1%. This indicated that even when considering extremely small droplets, their impact

on the results of this study was extremely limited.

5 Conclusions

The study investigated how droplet size, emission velocity, emission angle, distance between the HVE and the source, as well as suction flow rates of HVE affected its removal efficiency. Furthermore, it investigated how using HVE influenced FT. The following conclusions could be drawn.

The highest cumulative removal efficiency of HVE was observed for droplets generated by HATH (100%), followed by PJH (73.6%) and USI (60.9%). The velocity of the droplets emerged as a key factor affecting cumulative removal efficiency, with higher velocities corresponding to lower removal efficiency. Under equivalent conditions, the cumulative removal efficiencies for low-velocity (0.8 m/s), medium-velocity (3.4 m/s), and high-velocity droplets (6.0 m/s) were approximately 97.9%, 73.6%, and 58% respectively.

The removal efficiency of HVE increased as the emission angle decreased for an HVE with a diameter of 15 mm. Increasing the distance between HVE and the source only increased the removal efficiency. For example, when decreasing the distance from 4 cm to 1 cm, there was an increase in cumulative removal efficiency from 58.0% to 100% for high velocity (6.0 m/s) droplets. The suction flow rates of HVE had a limited impact on the cumulative removal efficiency. Increasing them from the standard value (250 l/min) to 350 l/min or decreasing them to 150 l/min led to an increase in the cumulative removal efficiency of droplets (6 m/s) from 58.0% to 59.2% or a decrease to 54.6%, respectively.

After using HVE, both the cumulative suspension fraction and cumulative deposition fraction experienced a significant reduction. However, the velocity of droplets remained the key factor affecting both the cumulative deposition fraction and suspension fraction when using HVE. Furthermore, compared to the background condition (without using HVE), the use of HVE could reduce FT by 68.0%-92.3%.

This study contributed to a better understanding of the removal efficiency of HVE in controlling splatter, providing practical recommendations for its use, and demonstrating that optimizing the suction flow rates might not be cost-effective. On the other hand, the study revealed limitations in the performance of HVE, specifically its limited control range and suboptimal efficiency in removing high-velocity droplets. This emphasized the necessity for developing new control measures that provided a wide control range and high efficiency in removing high-velocity droplets.

Acknowledgement

This study was supported by the Fundamental Research Funds for the Central Universities (No. 531118010378) and by the Natural Science Foundation of Hunan Province of China (No. 2023JJ30127).

Reference

[1] World Health Organization Infection prevention and control of epidemic-and pandemic-prone acute respiratory infections in health care. World Health Organization, (2014).
[2] World Health Organization Considerations for the provision of essential oral health services in the context of COVID-19. World Health Organization. (2020).
[3] J. Zhu, J. Guo, Y. Xu, et al. (2020). Viral dynamics of SARS-CoV-2 in saliva from infected patients. J Infect. 81 (3): e48-e50.
[4] Q. Yang, T. Saldi, P. Gonzales, et al. (2021). Just 2% of SARS-CoV-2-positive individuals carry 90% of the virus circulating in communities. Proc Natl Acad Sci USA. 118 (21): e2104547118.
[5] G. Kampf, D. Todt, S. Pfaender, et al. (2020). Persistence of coronaviruses on inanimate surfaces and their inactivation with biocidal agents. J Hosp Infect. 104 (3): 246-251.
[6] D. Chang, G. Mo, X. Yuan, et al. (2020). Time Kinetics of Viral Clearance and Resolution of Symptoms in Novel Coronavirus Infection. Am J Respir Crit Care Med. 201 (9): 1150-1152.
[7] L. Zou, F. Ruan, M. Huang, et al. (2020). SARS-CoV-2 Viral Load in Upper Respiratory Specimens of Infected Patients. N Engl J Med. 382 (12): 1177-1179.
[8] C. Zemouri, C. Volgenant, M. Buijs, et al. (2020). Dental aerosols: Microbial composition and spatial distribution. J Oral Microbiol. 12 (1): 1762040.
[9] X. Peng, X. Xu, Y. Li, et al. (2020). Transmission routes of 2019-nCoV and controls in dental practice. Int J Oral Sci. 12 (1): 9.
[10] B. Polednik. (2014). Aerosol and bioaerosol particles in a dental office. Environ Res. 134: 405-9.
[11] M. Razavi, Z. Butt, H. Chen, et al. (2021). In Situ Measurement of Airborne Particle Concentration in a Real Dental Office: Implications for Disease Transmission. Int J Environ Res Public Health. 18 (17): 8955.
[12] S. Al-Amad, M. Awad, F. Edher, et al. (2017). The effect of rubber dam on atmospheric bacterial aerosols during restorative dentistry. J Infect Public Health. 10 (2): 195-200.
[13] R. Rautemaa, A. Nordberg, K. Wuolijoki-Saaristo, et al. (2006). Bacterial aerosols in dental practice - a potential hospital infection problem? J Hosp Infect. 64 (1): 76-81.
[14] K. Ram, R. Thakur, D. Singh, et al. (2021). Why airborne transmission hasn't been conclusive in case of COVID-19? An atmospheric science perspective. Sci Total Environ. 773: 145525.
[15] M. Bazant, J. Bush. (2021). A guideline to limit indoor airborne transmission of COVID-19. Proc Natl Acad Sci U S A. 118 (17): e2018995118.
[16] H. Senpuku, M. Fukumoto, T. Uchiyama, et al. (2021). Effects of Extraoral Suction on Droplets and Aerosols for Infection Control Practices. Dent. J. 9 (7): 80.
[17] A. Iliadi, D. Koletsi, T. Eliades, et al. (2020). Particulate Production and Composite Dust during Routine Dental Procedures. A Systematic Review with Meta-Analyses.

Materials. 13 (11): 2513.
[18] J. Comisi, T. Ravenel, A. Kelly, et al. (2021). Aerosol and spatter mitigation in dentistry: Analysis of the effectiveness of 13 setups. J Esthet Restor Dent. 33 (3): 466-479.
[19] Q. Ou, R. Placucci, J. Danielson, et al. (2021). Characterization and mitigation of aerosols and spatters from ultrasonic scalers. J Am Dent Assoc. 152 (12): 981-990.
[20] A. Puljich, K. Jiao, R. Lee, et al. (2022). Simulated and clinical aerosol spread in common periodontal aerosol-generating procedures. Clin Oral Investig. 26 (9): 5751-5762.
[21] W. Remington, B. Ott, T. Hartka. (2022). Effectiveness of barrier devices, high-volume evacuators, and extraoral suction devices on reducing dental aerosols for the dental operator: A pilot study. J Am Dent Assoc. 153 (4): 309-318.e1.
[22] M. Fennelly, C. Gallagher, M. Harding, et al. (2022). Real-time Monitoring of Aerosol Generating Dental Procedures. J Dent. 120: 104092.
[23] M. Jacks. (2002). A laboratory comparison of evacuation devices on aerosol reduction. J Dent Hyg. 76 (3): 202-6.
[24] S. Harrel, J. Barnes, F. Rivera-Hidalgo. (1996). Reduction of aerosols produced by ultrasonic scalers. J Periodontol. 67 (1): 28-32.
[25] H. Akin, O. Karabay, H. Toptan, et al. (2022). Investigation of the Presence of SARS-CoV-2 in Aerosol After Dental Treatment. Int Dent J. 72 (2): 211-215.
[26] C. Yuan, H. Yang, S. Zheng, et al. (2023). Spatiotemporal distribution and control measure evaluation of droplets and aerosol clouds in dental procedures. Infect Control Hosp Epidemiol. 44 (3): 514-516.
[27] B. Barrett, J. McGovern, W. Catanzaro, et al. (2022). Clinical Efficacy of an Extraoral Dental Evacuation Device in Aerosol Elimination During Endodontic Access Preparation. J Endod. 48 (12): 1468-1475.
[28] N. Johnston, R. Price, C. Day, et al. (2009). Quantitative and qualitative analysis of particulate production during simulated clinical orthodontic debonds. Dent Mater. 25 (9): 1155-62.
[29] K. Ali, M. Raja. (2021). COVID-19: dental aerosol contamination in open plan dental clinics and future implications. Evid Based Dent. 22 (2): 54-55.
[30] R. Holliday, J. Allison, C. Currie, et al. (2021). Evaluating contaminated dental aerosol and splatter in an open plan clinic environment: Implications for the COVID-19 pandemic. J Dent. 105: 103565.
[31] B. Blackley, K. Anderson, F. Panagakos, et al. (2022). Efficacy of dental evacuation systems for aerosol exposure mitigation in dental clinic settings. J Occup Environ Hyg. 19 (5): 281-294.
[32] J. Holloman, S. Mauriello, L. Pimenta, et al. (2015). Comparison of suction device with saliva ejector for aerosol and spatter reduction during ultrasonic scaling. J Am Dent Assoc. 146 (1): 27-33.
[33] A. Onescu, E. Brambilla, L. Manzoli, et al. (2021). Efficacy of personal protective equipment against coronavirus transmission via dental handpieces. J Am Dent Assoc. 152 (8): 631-640.
[34] A. Ionescu, E. Brambilla, L. Manzoli, et al. (2021). Aerosols modification with HO reduces airborne contamination by dental handpieces. J Oral Microbiol. 13 (1): 1881361.
[35] D. Gheorghita, F. Szabó, T. Ajtai, et al. (2022). Aerosol Reduction of 2 Dental Extraoral Scavenger Devices In Vitro. Int Dent J. 72 (5): 691-697.
[36] X. Li, M. Mak, K. Ma, et al. (2021). Evaluating flow-field and expelled droplets in the mock-up dental clinic during the COVID-19 pandemic. Phys Fluids. 33 (4):

047111.
[37] E. Haffner, M. Bagheri, J Higham, et al. (2021). An experimental approach to analyze aerosol and splatter formations due to a dental procedure. Exp Fluids. 62 (10): 202.
[38] C. Xing, Z. Ai, Z. Liu, et al. (2024). Characteristics of droplets emission immediately around mouth during dental treatments. Build Environ. 248, 111066.
[39] F. Zhao. (2017). Oral Health Care. Shanghai: Fudan University Press.
[40] YY/T 0629-2021. (2021). Dentistry-Central suction source equipment. Pharmaceutical Industry Standards of the People's Republic of China. Beijing: Standards Press of China.
[41] E. Küçüktopcu, B. Cemek. (2019). Evaluating the influence of turbulence models used in computational fluid dynamics for the prediction of airflows inside poultry houses. Biosyst. Eng. 183: 1-12.
[42] K. Kwon, I. Lee, G. Zhang, et al. (2015). Computational fluid dynamics analysis of the thermal distribution of animal occupied zones using the jet-drop-distance concept in a mechanically ventilated broiler house. Biosyst. Eng. 136: 51-68.
[43] Ansys Academic Research Mechanical and CFD, “Realizable k-epsilon model,” in ANSYS Fluent Theory Guide (ANSYS, Inc., Canonsburg, PA, 2020f), R. 2.
[44] Y. Zhou, S. Ji. (2021). Experimental and numerical study on the transport of droplet aerosols generated by occupants in a fever clinic. Build Environ. 187: 107402.
[45] S. Balachandar. (2009). A scaling analysis for point–particle approaches to turbulent multiphase flows. Int. J. Multiphas. Flow. 35 (9): 801-810.
[46] S. Morsi, A. Alexander. (1972). An investigation of particle trajectories in two-phase flow systems. J. Fluid Mech. 55 (2): 193–208.
[47] L. Talbot, R. Cheng, R. Schefer. (1980). Thermophoresis of particles in a heated boundary layer. J. Fluid Mech. 101 (4): 737–758.
[48] P. Saffman. (2021). The lift on a small sphere in a slow shear flow. J. Fluid Mech. 22 (2): 385-400.
[49] Ansys Academic Research Mechanical and CFD, Fluent Theory Guide (ANSYS, Inc., Canonsburg, PA, 2020d), R.2.
[50] S. Sazhin. (2006). Advanced models of fuel droplet heating and evaporation. Prog. Energy Combust. Sci. 32 (2): 162–214.
[51] Y. Lu, Z. Lin. (2022). Coughed droplet dispersion pattern in hospital ward under stratum ventilation. Build Environ. 208, 108602.
[52] S. Basu, P. Kabi, S. Chaudhuri. (2020). Insights on drying and precipitation dynamics of respiratory droplets from the perspective of COVID-19. Phys. Fluids. 32 (12), 123317.
[53] M. Owen, D. Ensor. (1992). Airborne particle sizes and source found in indoor air Atmos. Environ. 26A (12): 2149-2162.
[54] X. Li, C. Mak, Z. Ai, et al. (2023). Cross-infection risk assessment in dental clinic: Numerical investigation of emitted droplets during different atomization procedures. Journal of Building Engineering. 75, 106961.
[55] Z. Zhang, Q. Chen. (2006). Experimental measurements and numerical simulations of particle transport and distribution in ventilated rooms. Atmospheric Environment. 40 (18): 3396-3408.
[56] X. Li, Y. Shang, Y. Yan, et al. (2018). Modelling of evaporation of cough droplets in inhomogeneous humidity fields using the multi-component Eulerian-Lagrangian approach. Build Environ. 128: 68-76.
[57] C. Xing, S. Zhang, M. Bai, et al. (2021). Spatiotemporal distribution of aerosols generated by using powder jet handpieces in periodontal department, Sustain. Cities

Soc. 75, 103353.
[58] C. Robertson, J. Clarkson, M. Aceves-Martins, et al. (2015). A review of aerosol generation mitigation in international dental guidance. Int Dent J. 72 (2): 203-210.
[59] X. Li, C. Mak, K. Ma, et al. (2021). Restoration of dental services after COVID-19: the fallow time determination with laser light scattering Sustain. Sustain Cities Soc. 74: 103134.
[60] Z. Liu, G. Yao, Y. Li, et al. (2021). Bioaerosol distribution characteristics and potential SARS-CoV-2 infection risk in a multi-compartment dental clinic. Build Environ. 225: 109624.